Physico-Mechanical Properties of Biodegradable Starch Nanocomposites

Nancy L. García, Laura Ribba, Alain Dufresne, Mirta I. Aranguren, Silvia Goyanes*

Nanocomposites of cassava starch reinforced with waxy starch nanocrystals were prepared. They showed a 380% increase of the rubbery storage modulus (at 50 °C) and a 40% decrease in the water vapor permeability. X-ray spectra show that the composite was more amorphous than the neat matrix, which was attributed to higher equilibrium water content in the composites. TGA confirmed this result and its thermal derivative suggested the formation of hydrogen bonding between glycerol and the nanocrystals. The reinforcing effect of starch nanocrystals was attributed to strong filler/matrix interactions due to the hydrogen bonding. The decrease of the permeability suggests that the nanocrystals were well dispersed, with few filler/filler interactions.

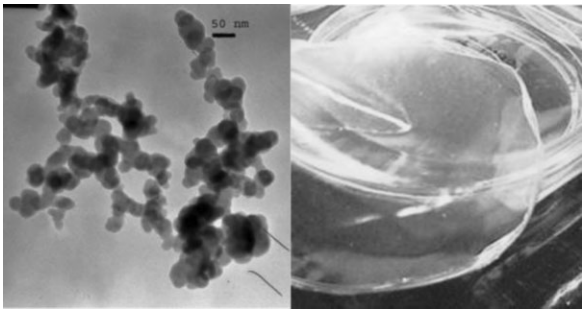

Introduction

Today's high-quality starches have evolved through the marriage of polymer chemistry and food science. This has arisen as a result of the broad range of starch applications, derived mainly from the emergence of a packaging industry and the increased availability of starch. Therefore, the increasing interest in starch as a potential replacement for conventional synthetic packaging materials, such as biodegradable films, is not surprising.

Cassava (*Manihot esculenta*), also called manioc, tapioca or yuca, is one of the most important food crops in the humid tropical countries, being particularly well-suited to conditions of low nutrient availability and able to survive drought.[1] Cassava starch can perform most of the functions for which maize, rice and wheat starch are currently used. Cassava starch is used in the manufacture of sweeteners, sizing of paper and textile and, in particular, it is used as an excellent thickener and stabilizer for foods. The currently increasing cassava production will lead to higher volume production of starch, making it cheaper for different industrial applications and allowing the opening of new markets. Being a pure renewable natural polymer, starch has already multiple applications.[2,3] Cassava starch, either natural or modified, has some inherent properties that are highly demanded in the food industry,

N. L. García, L. Ribba, S. Goyanes
Laboratorio de Polímeros y Materiales Compuestos, Dep. De Física, FCEN – UBA, Ciudad Universitaria, C1428EGA, Ciudad Autónoma de Buenos Aires, Argentina
Fax: + 54 11 4576 3357; E-mail: goyanes@df.uba.ar
N. L. García
Universidad Nacional de San Martín (UNSAM), Buenos Aires, Argentina
A. Dufresne
Grenoble Institute of Technology (INPG) The International School of Paper, Print Media and Biomaterials (PAGORA) – BP 65 – F-38402 Saint Martin d'Hères Cedex, France
M. I. Aranguren
INTEMA, Univ.
National de Mar del Plata, Av. Juan B. Justo 43027608FDQ, Mar del Plata, Argentina

DOI: 10.1002/mame.200800271

such as high transparency, which determines its suitability in the preparation of sauces for ready-to-eat foods, and high resistance to acidity, which allows its use in acid-based sauces and jams.

In recent years, starches alone or as part of a composite have been studied for their application in the film and packaging industry.[4–15] The formation of edible starch films involves gelatinization of starch granules by heating in excess water. This procedure results in granule swelling and disruption, as well as leaching of soluble components (amylose) from the granule. A viscous mass is obtained, consisting of a continuous phase constituted basically by solubilized amylose and a discontinuous phase of remnant granules, mainly based on amylopectin.[16] Cooling of the hot paste results in a viscoelastic gel. The formation of the junction zones (polymer molecules joined by covalent bonds, hydrogen bonding and/or Van der Waals' forces) of a gel can be considered to be the first stage of an attempt by starch molecules to crystallize. The collective processes that take part in the reduction of the solubility of dissolved starch are called retrogradation and involve the two constituent polymers, amylose and amylopectin, with amylose undergoing retrogradation at a much more rapid rate than amylopectin.

Cassava starch contains 72 wt.-% amylopectin and 28 wt.-% amylose (linear glucan with α-1,4-glycosidic linkages). Waxy maize starch, which is formed of nearly 100% amylopectin (a large, branched, D-glucopyranose polymer of starch containing both α-1,4 and α-1,6 linkages),[17] has built-in textural stability, due to the near absence of the more linear amylose molecule, and produces a clear and cohesive paste in foods. Waxy maize-starch nanocrystals, obtained by hydrolysis of native granules[18] have shown interesting reinforcing and barrier properties in different matrices.[19–21]

In this work, the physical and mechanical properties of a new nanocomposite type (plasticized cassava starch/maize starch nanocrystals) were studied and compared with those of the neat cassava starch films. The discussion was focused on the effect of the addition of the nanocrystals on the thermal degradation, mechanic dynamical properties, crystallinity of the cassava starch films, and the corresponding morphologies from the films cryo-fractured surfaces. The analysis of the films' behavior, including the kinetics of water absorption, considered also the chemical interactions observed by infrared spectroscopy.

Experimental Part

Cassava Starch Matrix

The cassava starch (72% amylopectin and 28% amylose) was provided by Bernesa S.A., Buenos Aires, Argentina. The plasticizer used was glycerol (Baker, purity 99.9%).

Waxy Starch Nanocrystals

Waxy maize-starch nanocrystals were obtained by acidic hydrolysis of 36.725 g of waxy maize starch (Waxylis, Roquette S. A., Lestrem, France) mixed in 250 mL of 3.16×10^{-3} M H_2SO_4, at 40 °C and 100 rpm, subjected to an orbital shaking action for 5 d. After that, the crystals were washed in distilled water and separated by successive centrifugations until neutrality was reached. They were stored at 4 °C with several drops of chloroform. The success of the hydrolysis in preparing the nanocrystals was confirmed by scanning and transmission electron microscopy.

Transmission Electron Microscopy (TEM)

Transmission electron micrographs of starch nanocrystals were taken with an EM 301 Philips transmission electron microscope at an acceleration voltage of 60 kV. A dilute starch nanocrystals suspension was sonicated for 10 min. After sonication, a drop of the starch nanocrystals suspension was deposited onto a carbon-coated microscopy grid and negatively stained with an aqueous 2% solution of uranyl acetate for 1 min. The liquid in excess was blotted with filter paper and the remaining liquid was dried before the specimen observation.

Field Emission Scanning Electron Microscopy (FE-SEM)

SEM, performed using a Zeiss DSM982 Gemini with a field emission gun (FEG), was used to examine the morphology of starch nanoparticles (previously lyophilized and sprinkled onto a conductive paper) as well as the cryogenic fractured surfaces of conformed films. In this last case, the samples were coated with a thin sputtered gold layer before analysis.

Processing of Films

Thermoplastic starch was processed by casting, from the mixing of native cassava-starch granules, glycerol and distilled water. A quantity of 15 g of a mixture of starch and glycerol (2:1 by weight) was dispersed in 185 g of distilled water. The mixture was heated from room temperature at a heating rate of $1.59\ ^\circ C \cdot min^{-1}$ under mechanical stirring for 28 minutes until gelatinization, which occurred at ≈70 °C. After gelatinization, the gel was degassed for 0.5 h with a vacuum mechanical pump. At that point, the composite films were prepared by adding the suspension of waxy maize starch nanocrystals in the desired quantities (2.5 wt.-% relative to the total mass, starch + plasticizer + nanocrystals). After that, the mixture was stirred for 10 min at 250 rpm and degassed for another 1 h. Then, the mixture was cast in a plastic mould and evaporated in a ventilated oven at 50 °C for 24 h. Solid films having a thickness between 300 and 400 μm were obtained.

Matrix and composite films were stored at 43% relative humidity (RH) (K_2CO_3 saturated solution) for 2 weeks before characterization and testing.

Polarized Light Microscopy

In order to determine the complete solubilization of starch, light microscopy photographs were taken with an Olympus BX60M optical microscope equipped with a color video camera using a

Macromol. Mater. Eng. 2009, 294, 169–177

Macromolecular Journals
DOI: 10.1002/mame.200800271

calibrated RS Image Olympus image system. Aliquots taken at different times of gelatinization were examined.

Attenuated Total Reflectance Fourier-Transform Infrared Spectroscopy (ATR FTIR)

Absorbance spectrum of the matrix and composite were recorded on a Genesis II Fourier-transform infrared spectrometer using the attenuate total reflectance (ATR) accessory. The spectra were obtained at a resolution of 2 cm^{-1} as the average of 32 scans.

X-Ray Diffraction

Matrix and composite films were submitted to X-ray radiation using a diffractometer, Philips model PW 1510, with a vertical goniometer operating at Cu K_α radiation wavelength ($\lambda = 1.542$ Å), 40 kV, 30 mA and sampling interval of 0.02°. Scattered radiation was detected in the angular range $2\theta = 10$–35°.

Thermogravimetric Analysis (TGA)

Thermogravimetric analysis was carried out for the matrix and the composite, using a Perkin-Elmer TGA-50H instrument under nitrogen atmosphere at 30 $mL \cdot min^{-1}$ and at a heating rate of 5 $°C \cdot min^{-1}$ from room temperature to 500 °C.

Dynamic Mechanical Analysis (DMA)

Dynamic mechanical measurements were performed for the matrix and composite, using a dynamic mechanical thermal analyzer (DMTA IV, Rheometric Scientific) in the rectangular tension mode at 1 Hz, in the temperature range −120 to +70 °C, a heating rate of 2 $°C \cdot min^{-1}$. The dimensions of the samples were $25 \times 9 \times 0.4$ mm^3. The samples were subjected to a cyclic strain lower than 0.04%. These strain values were sufficiently small to assure that the mechanical response of the specimen was within the linear viscoelastic range. The set up was used to determine the storage modulus E', the loss modulus E'' and the ratio of these two parameters, $\tan \delta = E''/E'$.

Water Absorption

The water absorption was determined for both the composite and the matrix. The samples used were thin rectangular films of $9 \times 11 \times 0.45$ mm^3. Samples were first dried overnight at 100 °C and under vacuum. After weighing to determine the initial weight (M_0), they were placed in a container conditioned at 98% RH using a saturated copper sulfate solution. At specific time intervals, the sample weight (M_t) was determined until an equilibrium value (M_∞) was reached. Three replicates were tested for the composite and for the matrix. The water content or water uptake of the samples was calculated by dividing the gain in weight ($M_t - M_0$) by the initial weight (M_0).

Water Vapor Permeability (WVP)

WVP tests were conducted according to ASTM E96-00.[22] Film specimens were conditioned for two weeks in desiccators at 25 °C and 43% RH (equilibrium with a K_2CO_3 saturated solution) before being analyzed. Each film sample was sealed over a circular opening of 21.85 mm in a permeation cell that was stored at 25 °C in desiccators. To maintain a 58% RH gradient across the film, silica gel (0% RH), activated at 200 °C, was placed inside the cell and a sodium bromide (NaBr) saturated solution (58% RH) was placed in the desiccators, outside the cell. Water vapor transport was determined from the weight gain of the permeation cell. After steady-state conditions were reached (about 2 h), eight weight measurements were made over 24 h. Changes in the weight of the cell were recorded to the nearest 0.0001 g and plotted as a function of time for 10 d. Cells were carefully shaken horizontally after every weighing. The slope of each line was calculated by linear regression ($r^2 > 0.99$) and the rate of water vapor transfer (WVT, $g \cdot h^{-1} \cdot m^{-2}$) was determined from the slope of the straight line ($g \cdot h^{-1}$) divided by the cell area (m^2). The thickness of each film was measured with a microscope at six randomly selected points after the permeation test. Three replicate samples were analyzed.

The WVP was calculated as:

$$WVP = [(WVT/S(R_1 - R_2)] \times T \quad (1)$$

where S is the saturation vapor pressure of water at the test temperature (25 °C), R_1 is the relative humidity in the desiccators, R_2 is the relative humidity inside the permeation cell, and T is the film thickness.

Results and Discussion

Morphology of the Starch Nanoparticles

Figure 1 shows a TEM micrograph of waxy starch nanoparticles. TEM was made using a drop of a suspension of the nanocrystals in water. As can be seen, nanocrystals have an average size below 50 nm and form aggregates of 1–5 μm, showing very close resemblance to the morphological characteristics previously reported[18,23] for pea-starch nanocrystals.

Figure 2 shows an FE-SEM micrograph of the lyophilized starch nanocrystals, illustrating the formation of laminar

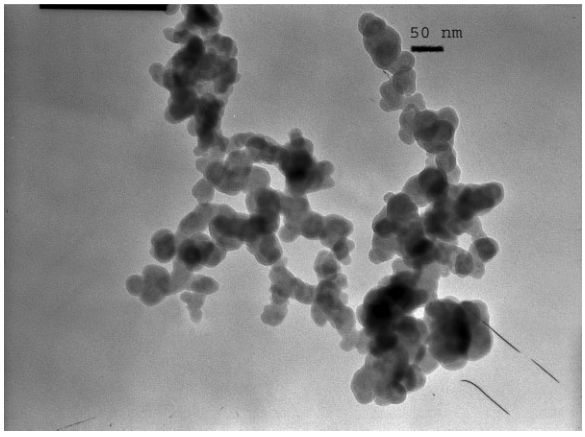

Figure 1. TEM of waxy maize-starch nanocrystals.

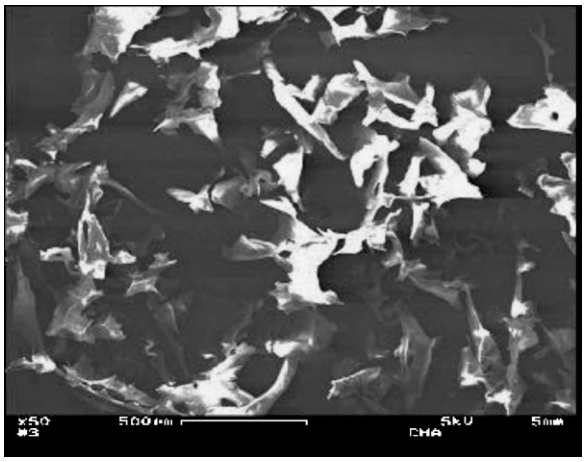

Figure 2. Scanning electron micrographs of lyophilized starch nanoparticles.

aggregates with large specific area, similar to the structures reported by Thielemans et al.[24] The existence of nanocrystals aggregates suggests the presence of a high number of OH-groups per individual nanocrystal, which become strongly associated by hydrogen bonding.

Gelatinization Process

The composite gelatinization process was followed by optical microscopy and the help of polarized light. Figure 3a–c shows a sequence of images registered during the gelatinization process, taken at 10 and 25 min, and at the end of the gelatinization (around 70 °C), respectively. After 10 min from setting the sample on the hot stage under the microscope, many Maltese cross shapes could still be observed (Figure 3a). This is a sign of the semi-crystalline character of the starch granules that leads to birefringence. As the process continued, the disruption of the semicrystalline structure of the granules began, decreasing the number of Maltese cross shapes observed (Figure 3b).[17] Finally, at the end of the gelatinization, the crosses disappeared completely from the resulting viscous solution (Figure 3c). This result allows us to infer that the nanocrystals are well-dispersed, or they are forming clusters with size below the optical resolution of the microscope employed (0.1 μm).

ATR FTIR

Figure 4a and b shows the FTIR spectra of the cassava starch film (matrix) and of the composite reinforced with 2.5 wt.-% nanocrystals in the regions 4 000–1 500, and 1 350–700 cm^{-1}, respectively.

The neat starch and composite films present similar features in the two FTIR spectral regions, with the exception of the peaks related to the absorptions of the hydroxyl groups, at 3 260, 1 650 and 1 015 cm^{-1}. As can be seen, the two bands at high wave numbers show a very slight broadening with the incorporation of starch nanoparticles, while the band at 1 015 cm^{-1}, associated with the C–OH bond, show notorious changes in the relative intensity of the doublet in agreement with the reports of Vicentini et al.[25] and Van Soest et al.[26] The slight broadening of the peaks, associated with OH-groups, suggests an increase in the number of oscillation modes, which could be associated with the presence of different types of hydrogen bonding interactions.

Although the FTIR spectra of composite and matrix show only slight differences, they were repeated in all the tests made on different samples. Additionally, similar effects have been reported[23] for PVA/pea starch nanocrystals.

X-Ray Diffraction

X-ray diffraction was used to investigate changes in the crystallinity of the cassava starch matrix due to the addition of 2.5 wt.-% nanocrystals. The patterns obtained

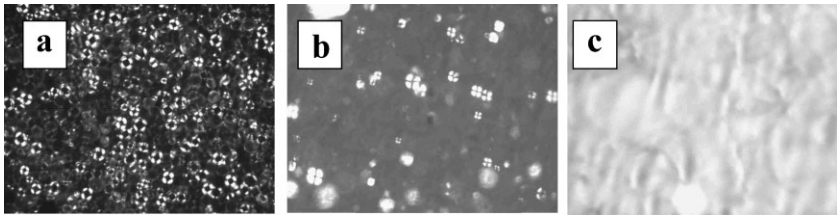

Figure 3. Light micrographs of Cassava starch during gelatinization at a) 10, b) 25 min, and c) the end of the gelatinization.

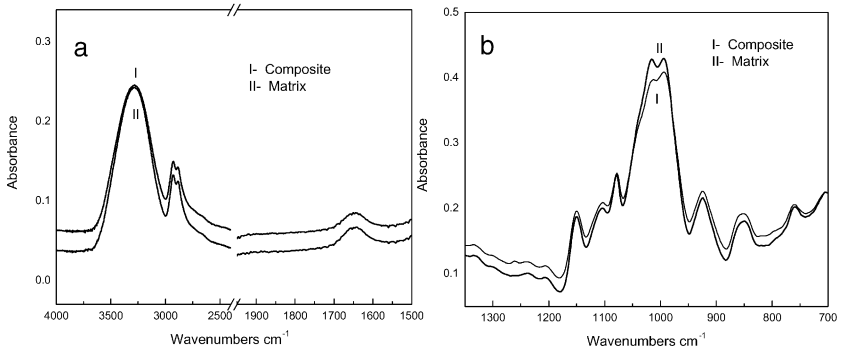

Figure 4. Infrared spectra in the spectral regions: a) 4 000–1 500 and b) 1 350–700 cm^{-1} for the composite (I) and matrix (II).

Macromol. Mater. Eng. **2009**, *294*, 169–177

Macromolecular Journals
DOI: 10.1002/mame.200800271

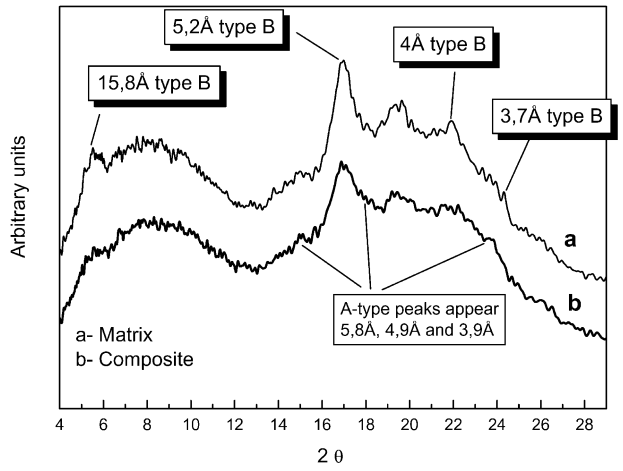

Figure 5. X-ray diffraction patterns of the matrix of plasticized cassava starch (a) and the composite of plasticized cassava/maize waxy nanocrystals (b).

for both films, matrix and composite, are shown in Figure 5.

The crystalline peaks were analyzed in the interval from $2\theta = 4$–30°, identifying the most intense peaks and calculating the distances between the planes of the crystals, d (Å), from the diffraction angles (°) according to Bragg's law: $n\lambda = 2d \sin\theta$, where λ is the wavelength of the X-ray beam and n is the order of reflection.

For the cassava-starch matrix (Figure 5), a contribution of the amorphous phase appears, containing in addition the diffraction of the B-V crystalline structure, with peaks at $2\theta = 5.6$, 17, 20, 22 and 24°, equivalent to d-spacings of 15.8, 5.2, 4.4, 4 and 3.7, respectively. In general, the diffraction of B-crystals is characterized by strong magnitude peaks at 5.6 and 17.1°, corresponding to an interplanar spacing $d = 15.7$ and 5.2 Å, respectively. This spectrum is in agreement with previous published results for cassava starch.[10–13,27]

Angellier et al.[21] reported the X-ray diffraction pattern for similar waxy maize starch nanocrystals (WN) and showed that they presented the A-type crystalline structure, characterized by two peaks at $2\theta = 10.1$ and 11.5°, a strong intensity peak at 15.3°, a double peak at 17.1 and 18.2°, and a last strong intensity peak at 23.5°. They also showed that, when adding starch nanocrystals to a thermoplastic waxy starch matrix, the typical peaks of the A-type crystals appear and the magnitude of the peaks increases with filler content, revealing that the crystalline structure of the starch nanocrystals is preserved. However, at 5 wt.-%, the lowest filler concentration used by these authors, the peaks associated to the type A pattern were not very prominent.

As can be seen in Figure 5, the addition of 2.5 wt.-% nanocrystals to the cassava matrix, leads to the reduction of B-V type peaks and to the very weak appearance of the A-type peaks.

A comparison between the two spectra shows that the composite is more amorphous than the neat starch. One of the reasons could be the higher water equilibrium content in the composites, as it will be discussed in the following sections.

Morphological Characterization by SEM

Figure 6a and b show the micrographs of the cryo-fractured surfaces of a neat Cassava starch film and a composite film containing 2.5 wt.-% nanocrystals, respectively. It can be observed that the surface of the neat starch (Figure 6a) is rough. This is similar to the results reported by Anglès and Dufresne[4] for a matrix of waxy starch plasticized with glycerol. The rough surface could be ascribed to the heterogeneous nature of this sample;[28] as was mentioned before, the matrix is a biphasic material composed of glycerol- and starch-rich phases.

When the nanocrystals are added to the matrix, the aspect of the fracture surface is quite different, as shown in Figure 6b. This is a smooth surface that contains a well-developed vein pattern, a feature usually found when the deformation of a composite is controlled by that of its amorphous homogeneous matrix. Similar results have been reported for other types of starch nanocomposites plasticized with glycerol.[4,29] The smooth fracture surface is associated with a homogeneous material.[28,30] Therefore, the results of the morphological characterization suggest that the glycerol is more homogeneously distributed in the case of the nanocomposite than in the case of the matrix. The nanocrystals probably interact with

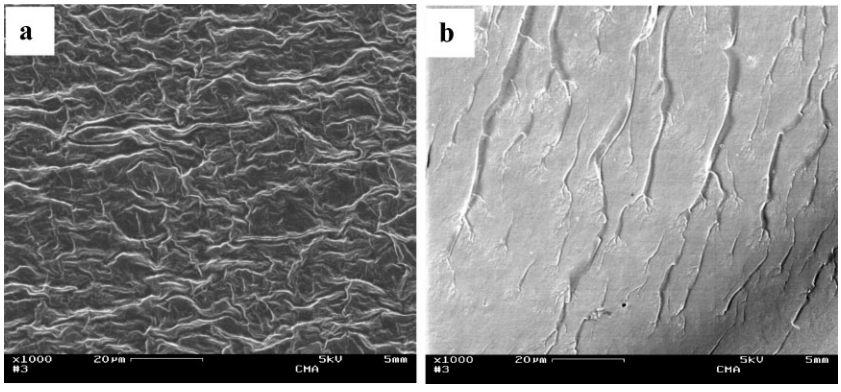

Figure 6. SEM images of the cryo-fracture surfaces of a) the neat cassava starch film, and b) the composite.

Table 1. Mass loss as determined from the thermogravimetric curves for glycerol-plasticized cassava starch and cassava starch/ waxy maize starch nanocrystals composite film.

Film	Mass loss %		
	First step	Second step	Third step
matrix	17.14	54.32	10.63
composite film (2.5 wt.-% nanocrystals)	21.39	51.14	9.16
matrix (dry basis)	–	65.56	12.83
composite film, (2.5 wt.-% nanocrystals), dry basis)	–	65.06	11.65

glycerol molecules, by hydrogen bonding, which leads to a more homogeneous distribution of the remaining (and reduced) concentration of glycerol.

Thermogravimetric Analysis TGA

The thermal decomposition process of the matrix and of the composite presents three main stages of reaction, which agree with previous reports.[29,31–33]

The first stage corresponds to the loss of water, the second stage is due to the decomposition of the glycerol-rich phase, and the third stage corresponds to the oxidation of the partially decomposed starch.

The thermogravimetric curves (TG and dTG) are shown in Figure 7a and b. The TG thermal derivate (dTG) curves show that, in the case of the neat starch film, a wide peak appears around 113 °C, which can be associated with the maximum in the water loss rate, while in the case of the composite the maximum is not observed. Moreover, both dTG signals show two overlapping peaks: one around 240 °C, probably associated with the decomposition of the glycerol-rich phase and another around 290 °C, associated with the degradation of the starch-rich phase. Notice that, in the case of the composite, the peaks appear to be slightly more overlapped. This result agrees with the FTIR spectroscopy results with regard to the presence of hydrogen bonding (glycerol-nanocrystals) in the composite and the reduced phase separation observed by SEM.

Table 1 summarizes the quantitative information on the thermal degradation occurring in each stage: in the first step, the starch/nanocrystals composite film shows a higher water content with respect to the neat starch matrix, which indicates an increased availability of OH-groups (probably arising from the starch matrix) ready for the formation of hydrogen bonding with the absorbed water. The mass lost in the other steps is similar for both systems (see dry basis results).

Dynamic Mechanical Analysis (DMA)

Figure 8 presents the isochronal evolution (1 Hz) with the temperature of the loss tangent tan δ, and the relative logarithm of the storage modulus (E'/E'_g), defined as the ratio between the actual modulus and the modulus in the glassy state, for biofilms of neat Cassava starch and the 2.5 wt.-% nanocrystal-reinforced composite.

The results show that the magnitude of the storage modulus increases when nanocrystals are incorporated to the starch. The rubbery storage modulus value measured at 50 °C increases from 3.80×10^7 Pa for the matrix to 1.47×10^8 Pa for the composite.

In Figure 8, two peaks are observed: the first around −60 °C and the second, wide and of low intensity, between −20 and 60 °C. According to the literature,[28,29,34] the starch-glycerol is a partially miscible system, in which two phases can be observed: one, rich in glycerol, relaxation of which occurs around −60 °C; and the other, rich in starch, appearing at higher temperatures. Mathew and Dufresne,[28] report a relaxation peak around 0 °C, which was associated with a rearrange-

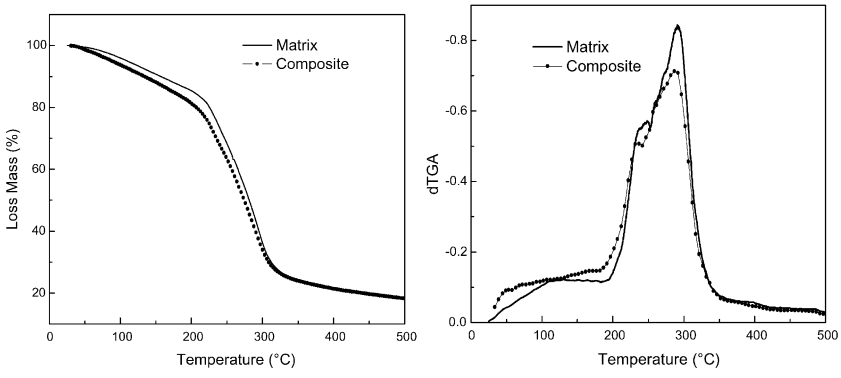

Figure 7. a) TGA, and b) dTG curves for a film of plasticized Cassava starch and the composite of plasticized Cassava/maize waxy nanocrystals.

Macromol. Mater. Eng. **2009**, *294*, 169–177

DOI: 10.1002/mame.200800271

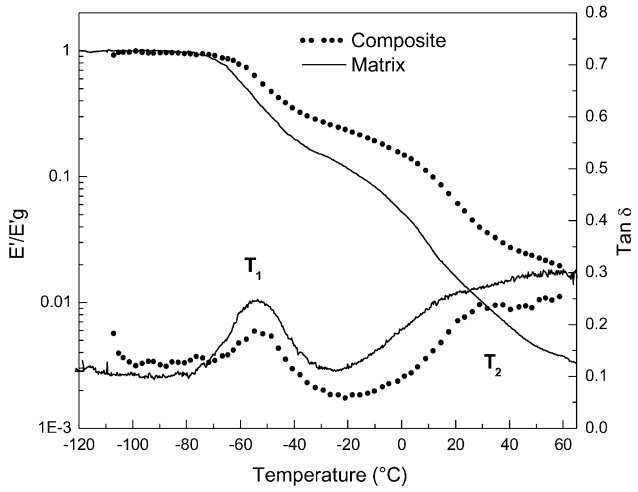

Figure 8. Evolution of the dynamic mechanical properties of the neat film and the composite with temperature. E'_g is the value of the storage modulus in the glassy state

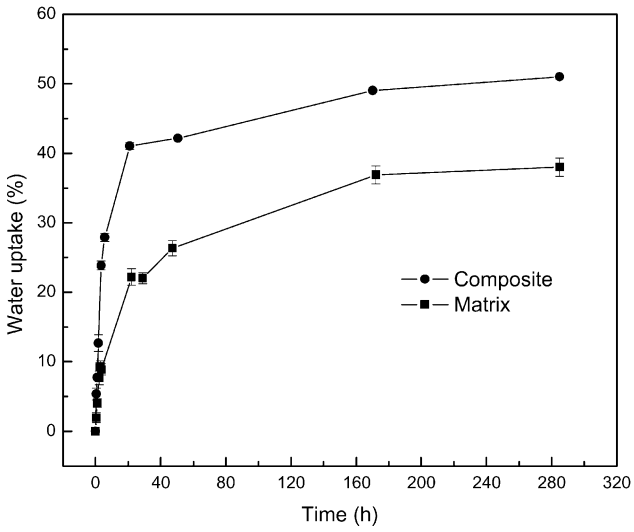

Figure 9. Water uptake during conditioning at 98% RH versus time for plasticized Cassava starch film and composite of plasticized Cassava/ maize waxy nanocrystals. The solid lines serve to guide the eye.

ment of amorphous starch chains in the presence of moisture. This phenomenon, known as retrogradation, is favored by the plasticizing effect of water. Therefore, taking into account that the TGA results showed higher water content in the composite than in the unfilled starch film, a clearer second relaxation peak was to be expected in the tan δ curve of the composite, as compared to that of the neat sample. This feature is marked as T_2 in Figure 8, where a better-defined peak appears in this temperature range. The relaxation associated with the glycerol-rich phase shifts slightly to higher temperatures, widens and diminishes its intensity and is more asymmetric with the nanocrystal addition. This result suggests that the presence of nanocrystals contributed to the establishment of hydrogen bonding between glycerol and starch nanocrystals. This idea is in good agreement with the results obtained from TGA, FTIR spectroscopy and FE-SEM when nanocrystals were incorporated.

Water Absorption

The water uptake of previously dried samples and after conditioning at 98% RH and 25 °C was plotted as function of time (Figure 9). All samples absorbed water during the experiment. Two stages were observed for both matrix and composite. At lower times, below 20 h, the absorption kinetics is fast, whereas after that, a slower absorption process follows leading to a plateau, which corresponds to the water uptake at equilibrium. Experiments were left up to 30 d to confirm equilibration. This behavior is in agreement with the observation reported by Kristo and Biliaderis.[27] In Figure 9, it can be also observed that, when the starch nanocrystal content is 2.5 wt.-%, more water is absorbed than for the unfilled starch. The equilibrium water uptake is around 50% for the composite and around 35% for the unfilled starch film.

From the TGA and DMA analysis, it was concluded that glycerol interacts with the nanocrystals through H-bonding with the OH-groups. The nanocrystals are mainly the crystalline zones of hydrolysis of waxy starch (99% amylopectin) and, therefore, have a large number of OH-groups in their surfaces. The results from the different tests show that these groups associate with glycerol molecules more than the cassava starch. This leads to a cassava starch matrix with more OH-groups available to interact with moisture, as compared to the unfilled film, which explains the experimental observation.

Water Vapor Permeability

The WVP values of the studied films are given in Table 2. The WVP values obtained for cassava-starch films are in agreement with previously reported values[10] and are of

Table 2. Water vapor permeability for cassava and cassava composite films.

Film	WVP (0/58% RH)
	$10^{10}\ g \cdot m^{-1} \cdot s^{-1} \cdot Pa^{-1}$
unfilled Cassava starch	4.5 ± 0.6
cassava starch with 2.5 wt.-% nanocrystals	2.7 ± 0.7

the same order of magnitude as those obtained from other biodegradable films, such as wheat gluten plasticized with glycerol (7×10^{-10} g · m^{-1} · s^{-1} · Pa^{-1}), amylose (3.80×10^{-10} g · m^{-1} · s^{-1} · Pa^{-1}).[35]

Table 2 shows that the permeability to the water vapor decreases by 40% for cassava starch filled with only 2.5 wt.-% starch nanocrystals. The presence of nanocrystals introduced a tortuous route for the molecule of water to pass through the films. The high efficiency in reducing moisture permeability, in spite of the low nanocrystal concentration, is due to its nanometric size. According to the model of the "winding way", the addition of nanocrystals hinders diffusion, generating a reduction in the permeability of the film to the water vapor.[36]

Conclusion

A nanocomposite film was obtained using starch nanocrystals prepared by acid hydrolysis of waxy maize starch granules as the reinforcing phase and cassava starch plasticized with glycerol as the matrix. The content of the platelet-like nanoparticles, around 50 nm in lateral size, was fixed at 2.5 wt.-%. After mixing the cassava-starch solution and the nanoparticle aqueous dispersion at 70 °C, solid nanocomposite films were obtained by casting and evaporating the water at 50 °C. The ensuing films were conditioned at 43% RH before testing. The properties of these nanocomposite films were compared to those of the unfilled matrix. All the results led to the conclusion that the addition of starch nanocrystals within the starchy matrix leads to a relocation of the main plasticizer, viz. glycerol. This means that specific interactions are likely to occur between the starch nanoparticles and glycerol. One of the consequences of this relocation is a slightly lower glycerol content of the cassava starch matrix compared to the neat polymer, leading to a slight increase of the temperature position of the main relaxation process associated with the glass transition of glycerol-rich domains. This results in a more amorphous state and higher water content of the plasticized starch film when adding starch nanocrystals. The presence of starch nanocrystals also leads to a substantial increase of the stiffness of the material, the modulus at 50 °C increasing by a factor close to 4, and a significant improvement of its barrier properties, the water vapour permeability decreasing by 40%.

Acknowledgements: We acknowledge financial support from the *Universidad de Buenos Aires, Consejo Nacional de Investigaciones Científicas y Técnicas de la República Argentina, Agencia Nacional de Investigaciones Científicas y Tecnológicas de la República Argentina* and the scientific program of cooperation between the *Ministry of Science, Technology and Productive Innovation of the Argentine Republic (MINCYT)* and the *ECOS-Sud of France*.

Received: August 29, 2008; Revised: November 18, 2008; Accepted: November 20, 2008; DOI: 10.1002/mame.200800271

Keywords: biofilms; DMA; nanocomposites; SEM; starch nanocrystals

[1] M. M. Burrell, *J. Exp. Bot.* **2003**, *54*, 451.
[2] International Starch Institute, Science Park Aarhus, Denmark 1999–2001; http://www.starch.dk/isi/starch/tmstarch.htm; Accessed January **2008**.
[3] N. J. Tonukari, *Electron. J. Biotechnol.* **2004**, *7*, available from: http://www.ejbiotechnology.info/content/vol7/issue1/issues/2/, Accessed January **2008**.
[4] M. N. Angles, A. Dufresne, *Macromolecules* **2000**, *33*, 8344.
[5] M. N. Angles, A. Dufresne, *Macromolecules* **2001**, *34*, 2921.
[6] S. Bhatnagar, M. A. Hanna, *Starch – Stärke* **1996**, *48*, 94.
[7] A. J. F. Carvalho, A. A. S. Curvelo, J. A. M. Agnelli, *Carbohydr. Polym.* **2001**, *45*, 189.
[8] A. Dufresne, M. R. Vignon, *Macromolecules* **1998**, *31*, 2693.
[9] A. Dufresne, D. Dupeyre, M. R. Vignon, *J. Appl. Polym. Sci.* **2000**, *76*, 2080.
[10] L. Famá, A. M. Rojas, S. Goyanes, L. Gerschenson, *LWT* **2005**, *38*, 631.
[11] L. Famá, S. K. Flores, L. Gerschenson, S. Goyanes, *Carbohydr. Polym.* **2006**, *66*, 8.
[12] L. Famá, S. Goyanes, L. Gerschenson, *Carbohydr. Polym.* **2007**, *70*, 265.
[13] S. K. Flores, L. Famá, A. M. Rojas, S. Goyanes, L. Gerschenson, *Food Res. Int.* **2007**, *40*, 257.
[14] M. García, M. Martino, N. Zaritzky, *J. Sci. Food Agric.* **1998**, *76*, 411.
[15] H. M. Park, W. K. Lee, C. Y. Park, W. J. Cho, C. S. Ha, *J. Mater. Sci.* **2003**, *38*, 909.
[16] H. F. Zobel, "Starch granule structure", in: *Developments in carbohydrate chemistry*, R. J. Alexander, H. F. Zobel, Eds., The American Association of Cereal Chemists, St. Paul 1994, pp. 1–36.
[17] D. J. Thomas, W. A. Atwell, "*Starche*", Eagan Press Handbook Series, St. Paul 1997, pp. 1–11.
[18] H. Angellier, L. Choisnard, S. Molina-Boisseau, P. Ozil, A. Dufresne, *Biomacromolecules* **2004**, *5*, 1545.
[19] H. Angellier, S. Molina-Boisseau, L. Lebrun, A. Dufresne, *Macromolecules* **2005**, *38*, 3783.
[20] H. Angellier, S. Molina-Boisseau, A. Dufresne, *Macromolecules* **2005**, *38*, 9161.
[21] H. Angellier, S. Molina-Boisseau, P. Dole, A. Dufresne, *Biomacromolecules* **2006**, *7*, 531.
[22] ASTM, "*Standard test methods for water vapor transmission of material, E96–00*", Annual book of ASTM, American Society for Testing and Materials, Philadelphia 1996.
[23] Y. Chen, X. Cao, P. Chang, M. Huneault, *Carbohydr. Polym.* **2008**, *73*, 8.
[24] W. Thielemans, M. N. Belgacem, A. Dufresne, *Langmuir* **2006**, *22*, 4804.
[25] N. M. Vicentini, N. Dupuy, M. Leitzelman, M. P. Cereda, P. J. A. Sobral, *Spectrosc. Lett.* **2005**, *38*, 749.
[26] J. J. G. Van Soest, H. Tournois, D. de Wit, J. F. G. Vliegenthart, *Carbohydr. Res.* **1995**, *279*, 201.
[27] E. Kristo, C. G. Biliaderis, *Carbohydr. Polym.* **2007**, *68*, 146.
[28] A. P. Mathew, A. Dufresne, *Biomacromolecules* **2002**, *3*, 1101.

[29] H. M. Wilhelm, M. R. Sierakowski, G. P. Souza, F. Wypych, *Carbohydr. Polym.* **2003**, *52*, 101.
[30] A. L. Da Róz, A. J. F. Carvalho, A. Gandini, A. A. S. Curvelo, *Carbohydr. Polym.* **2006**, *63*, 417.
[31] W. Jiang, J. Qiao, K. Sun, *Carbohydr. Polym.* **2006**, *65*, 139.
[32] A. Rajan, V. S. Prasad, T. E. Abraham, *Int. J. Biol. Macromol.* **2006**, *39*, 265.
[33] S. K. Rath, R. P. Singh, *J. Appl. Polym. Sci.* **1998**, *70*, 1795.
[34] A. A. S. Curvelo, A. J. F. Carvalho, J. A. M. Agnelli, *Carbohydr. Polym.* **2001**, *45*, 183.
[35] V. D. Alves, S. Mali, A. Beléia, M. V. E. Grossmann, *J. Food Eng.* **2007**, *78*, 941.
[36] J. C. Matayabas, S. R. Turner, "Nanocomposite technology for enhancing the gas barrier of polyethylene terephthalate", in: *Polymer-clay nanocomposites*, T. J. Pinnavaia, G. W. Beall, Eds., John Wiley & Sons, Chichester 2000, Chapter 11, pp. 207–225.